

VERY EARLY ULTRAVIOLET AND OPTICAL OBSERVATIONS OF THE TYPE IA SUPERNOVA 2009ig

RYAN J. FOLEY^{1,2}, P. J. CHALLIS¹, A. V. FILIPPENKO³, M. GANESHALINGAM³, W. LANDSMAN⁴, W. LI³, G. H. MARION¹, J. M. SILVERMAN³, R. L. BEATON⁵, V. N. BENNERT⁶, S. B. CENKO³, M. CHILDRESS^{7,8}, P. GUHATHAKURTA⁹, L. JIANG¹⁰, J. S. KALIRAI¹¹, R. P. KIRSHNER¹, A. STOCKTON¹², E. J. TOLLERUD¹³, J. VINKÓ^{14,15}, J. C. WHEELER¹⁵, AND J.-H. WOO¹⁶

Draft version November 2, 2011

ABSTRACT

Supernova (SN) 2009ig was discovered 17 hours after explosion by the Lick Observatory Supernova Search, promptly classified as a normal Type Ia SN (SN Ia), peaked at $V = 13.5$ mag, and was equatorial, making it one of the foremost supernovae for intensive study in the last decade. Here, we present ultraviolet (UV) and optical observations of SN 2009ig, starting about 1 day after explosion until around maximum brightness. Our data include excellent UV and optical light curves, 25 pre-maximum optical spectra, and 8 UV spectra, including the earliest UV spectrum ever obtained of a SN Ia. SN 2009ig is a relatively normal SN Ia, but does display high-velocity ejecta — the ejecta velocity measured in our earliest spectra ($v \approx -23,000$ km s⁻¹ for Si II $\lambda 6355$) is the highest yet measured in a SN Ia. The spectral evolution is very dramatic at times earlier than 12 days before maximum brightness, but slows after that time. The early-time data provide a precise measurement of 17.13 ± 0.07 days for the SN rise time. The optical color curves and early-time spectra are significantly different from template light curves and spectra used for light-curve fitting and K -corrections, indicating that the template light curves and spectra do not properly represent all Type Ia supernovae at very early times. In the age of wide-angle sky surveys, SNe like SN 2009ig that are nearby, bright, well positioned, and promptly discovered will still be rare. As shown with SN 2009ig, detailed studies of single events can provide significantly more information for testing systematic uncertainties related to SN Ia distance estimates and constraining progenitor and explosion models than large samples of more distant SNe.

Subject headings: supernovae — general; supernovae — individual (SN 2009ig)

1. INTRODUCTION

Type Ia supernovae (SNe Ia) are exceptionally good distance indicators, allowing precise measurements of various cosmological parameters, including the first significant constraints on Ω_Λ (e.g.,

Riess et al. 1998; Perlmutter et al. 1999; Riess et al. 2007; Wood-Vasey et al. 2007; Hicken et al. 2009; Kessler et al. 2009; Amanullah et al. 2010; Conley et al. 2011; Suzuki et al. 2011). The progenitor system and explosion mechanism are generally known (a thermonuclear explosion of a C/O white dwarf (WD) in a binary system; Hoyle & Fowler 1960; Colgate & McKee 1969; Nomoto et al. 1984; Woosley et al. 1986), but the specifics of the various models — such as whether the progenitor comes from a single- or double-degenerate system — are ill constrained (e.g., Hillebrandt & Niemeyer 2000; Howell 2011). Many studies of individual peculiar SNe Ia, which can probe the extremities of the models or show what a normal SN Ia is *not*, have been conducted over the years (e.g., Li et al. 2001, 2003; Hamuy et al. 2003; Howell et al. 2006; Foley et al. 2009, 2010), but intense studies of individual normal SNe Ia are relatively rare. Systematic studies of large samples of normal SNe Ia can provide important constraints for the models, but extremely detailed observations of even a single normal object can be as constraining as hundreds of objects with much lower quality data.

The ultraviolet (UV) portion of a SN Ia spectral energy distribution (SED) provides a bounty of information about the explosions of SNe Ia. UV spectra are the most constraining data for determining the effects of temperature, density, and nonthermal ionization (e.g., Höflich et al. 1998; Lentz et al. 2001). SN Ia UV spectra are dominated by a forest of overlapping lines from Fe-group elements. UV photons are repeatedly absorbed and re-emitted in those lines and gradually scattered redward where lower opacities allow them to escape. There-

¹ Harvard-Smithsonian Center for Astrophysics, 60 Garden Street, Cambridge, MA 02138, USA.

² Clay Fellow. Electronic address rfoley@cfa.harvard.edu.

³ Department of Astronomy, University of California, Berkeley, CA 94720-3411, USA.

⁴ NASA Goddard Space Flight Center, Greenbelt, MD 20771, USA.

⁵ Department of Astronomy, University of Virginia, Charlottesville, VA 22904-4325, USA.

⁶ Department of Physics, University of California, Santa Barbara, CA 93106-9530, USA.

⁷ Physics Division, Lawrence Berkeley National Laboratory, 1 Cyclotron Road, Berkeley, CA 94720, USA.

⁸ Department of Physics, University of California, 366 LeConte Hall, Berkeley, CA 94720-7300, USA.

⁹ UCO/Lick Observatory, University of California, Santa Cruz, CA 95064, USA.

¹⁰ Steward Observatory, University of Arizona, 933 North Cherry Avenue, Tucson, AZ 85721, USA.

¹¹ Space Telescope Science Institute, 3700 San Martin Drive, Baltimore, MD 21218, USA.

¹² Institute for Astronomy, University of Hawaii, Honolulu, HI 96822, USA.

¹³ Center for Cosmology, Department of Physics and Astronomy, 4129 Frederick Reines Hall, University of California, Irvine, CA 92697, USA.

¹⁴ Department of Optics & Quantum Electronics, University of Szeged, Dóm tér 9, Szeged H-6720, Hungary.

¹⁵ Astronomy Department, University of Texas, Austin, TX 78712, USA.

¹⁶ Astronomy Program, Department of Physics and Astronomy, Seoul National University, Seoul, 151-742, Korea.

fore, the UV is crucial to the formation of the optical SED of SNe Ia (Sauer et al. 2008) and extremely sensitive to both the progenitor composition and explosion mechanism. Observations of the UV directly probe the composition of the outermost layers of ejecta which are transparent at optical wavelengths soon after explosion. Furthermore, Kasen (2010) showed that single-degenerate progenitor systems should have strong UV emission at early times from the SN ejecta interacting with the companion star; therefore, early UV observations directly test progenitor models.

At optical wavelengths SNe Ia are remarkably uniform in luminosity ($\sigma \approx 0.16$ mag; Mandel et al. 2011), after correcting for light-curve shape and color. This relationship extends to the U band and UV, but with larger scatter (Jha et al. 2006; Brown et al. 2010). The scatter in the optical can be further reduced if one accounts for the correlation between intrinsic color and ejecta velocity (Foley & Kasen 2011). Along with the observed $B - V$ color of SNe Ia (Pignata et al. 2008; Wang et al. 2009a), their intrinsic $B - V$ color correlates strongly with velocity, with intrinsically redder objects having high velocity (Foley & Kasen 2011; Foley et al. 2011). This is explained as additional line blanketing in the B band of the high-velocity objects, and this trend should extend to the UV (Foley & Kasen 2011). Ganeshalingam et al. (2011) found that higher-velocity SNe Ia tend to have faster B -band rise times than lower-velocity SNe Ia ($\Delta t = 1.4$ days), but this is not the case for V -band rise times.

SNe Ia bright enough to be observed by the *International Ultraviolet Explorer* (*IUE*) were rare (Foley et al. 2008), and only one object has a published high signal-to-noise ratio (S/N) *Hubble Space Telescope* (*HST*) spectrum near maximum light covering wavelengths $\lesssim 2900$ Å: SN 1992A (Kirshner et al. 1993), observed nearly two decades ago. *Swift* has obtained spectra of several SNe Ia, but because of typically short exposure times, they are generally of poor quality (Bufano et al. 2009). In Cycle 17, *HST* obtained a single spectrum of 30 SNe Ia (GO-11721; PI Ellis); however, because of the choice of grating, these spectra do not probe wavelengths shorter than ~ 2900 Å (Cooke et al. 2011). In total, there have been 7 SNe Ia with published premaximum spectra probing wavelengths shortward of ~ 2900 Å (SNe 1980N, 1986G, 1989B, 1990N, 1991T, 1992A, and 2005cf; Jeffery et al. 1992; Kirshner et al. 1993; Foley et al. 2008; Bufano et al. 2009).

SN 2009ig was discovered at an unfiltered magnitude of 17.5, 4 mag below peak, on 2009 August 20.48 (UT dates are used throughout this paper) by Kleiser et al. (2009) during the Lick Observatory Supernova Search (LOSS) with the 0.76 m Katzman Automatic Imaging Telescope (KAIT; Filippenko et al. 2001). There was no object detected on 2009 August 16.46 to a limit of 18.7 mag. It was discovered in NGC 1015, an SBa galaxy at $cz = 2629$ km s $^{-1}$ (Wong et al. 2006) with distance $D = 33.1$ Mpc ($\mu = 32.6 \pm 0.4$ mag) from a Tully-Fisher measurement (Tully 1988).

Navasardyan et al. (2009) obtained an optical spectrum of SN 2009ig on 2009 August 21.08, only 0.7 days after discovery, and determined that it was a young SN Ia. Clearly, SN 2009ig was discovered very shortly after explosion. We triggered multiple programs to study the

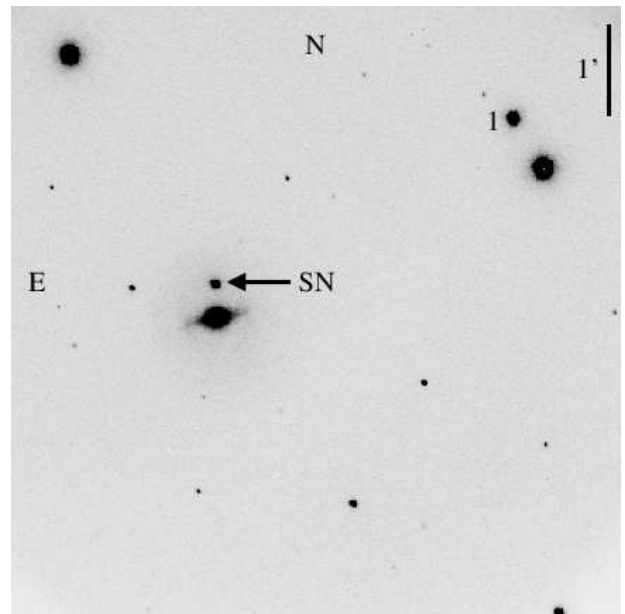


FIG. 1.— KAIT R -band image of SN 2009ig and its host galaxy, NGC 1015. The field of view (FOV) is $6.7' \times 6.7'$. The SN and comparison star are marked.

photometric and spectroscopic evolution of the object, its circumstellar environment, its spectropolarimetry, its energetics, and other aspects. Here we focus on the early-time UV and optical SN spectroscopy and photometry.

We present our UV and optical data in Section 2, and derive basic maximum-light parameters for SN 2009ig in Section 3. The UV spectra are discussed in Section 4. In Section 5 and Section 6, we compare the early-time photometry and spectroscopy, respectively, to that of other objects and to models. We discuss our findings and summarize our conclusions in Section 7.

2. OBSERVATIONS AND DATA REDUCTION

2.1. Optical and Ultraviolet Photometry

Broad-band $BVRI$ photometry of SN 2009ig was obtained using KAIT with the KAIT4 filters set (Ganeshalingam et al. 2010) at Lick Observatory starting on 21.5 August 2009 (about two weeks before maximum light). Within a day of the discovery of SN 2009ig, KAIT was programmed to observe the field with a nightly cadence to sample the rise and maximum of the light curves. Two weeks after maximum light the cadence was changed to every 3–4 days. In total, we have 55 photometry epochs. A finder chart of SN 2009ig, its host galaxy, and a comparison star is shown in Figure 1.

The data were reduced using a mostly automated pipeline developed for KAIT images (Ganeshalingam et al. 2010). Images were bias-corrected and flatfielded at the telescope. Using galaxy templates obtained a year and a half after discovery, the data images were galaxy subtracted to remove galaxy flux at the position of the SN. The flux of the SN and the local field star were measured using the point-spread function (PSF) fitting photometry package DAOPHOT in IRAF¹⁷. Instrumental magnitudes were color-corrected to the Landolt (1992) system using the

¹⁷ IRAF: The Image Reduction and Analysis Facility is distributed by the National Optical Astronomy Observatory, which is

average color terms measured on multiple photometric nights as presented by Ganeshalingam et al. (2010). The magnitudes of the local field standard were calibrated against Landolt (1992) standards on seven photometric nights.

The field of SN 2009ig suffers from a dearth of local standards that are bright enough to measure reliably, but not so bright that they saturate the detector. After trying combinations of available standards, we find that the smoothest, most believable light curves are obtained using a single, bright comparison star whose photometry is given in Table 1. We caution that this leaves our final light curves susceptible to a systematic offset from an incorrect determination of the Landolt magnitude of the comparison star, but should not change the overall shape of our light curves. KAIT photometry of SN 2009ig is presented in Figure 2 and Table 2.

The *Swift* team initiated target-of-opportunity observations of SN 2009ig with the Ultraviolet/Optical Telescope (UVOT; Roming et al. 2005) and the X-ray Telescope (XRT; Burrows et al. 2005) onboard the *Swift* gamma-ray burst satellite (Gehrels et al. 2004) beginning 2009 August 21.8. We performed digital image subtraction on all of the UVOT data using the final epoch as a template to remove host-galaxy contamination with the ISIS software package (Alard 2000). The *U*-, *B*-, and *V*-band data were then reduced using the calibration technique described by Li et al. (2006), while $[UVW2]$, $[UVM2]$, and $[UVW1]$ (corresponding to central/effective wavelengths of 1941/3064, 2248/2360, and 2605/3050 Å, respectively; Brown et al. 2010) photometry was obtained using the zeropoints from Poole et al. (2008).

The three bluest UVOT filters all have a significant wing that extends to optical wavelengths. This “red leak” is particularly problematic for SNe Ia, which have SEDs that peak in the optical and significantly depressed UV flux relative to the optical flux. As a result, a significant fraction of the flux measured in the UV filters comes from the optical portion of the SED. Brown et al. (2010) provides red-leak corrections for the UVOT filters. However, these corrections were calculated from the $t = +5$ day SN 1992A spectrum, which is the single published high S/N UV near-maximum SN Ia spectrum (Kirshner et al. 1993). SN Ia SEDs evolve with time, and especially quickly for the phases we examine here. We therefore do not want to make a single correction to our data. Unfortunately, there are no other suitable, published SN Ia spectra from which we could make red-leak corrections. As a result, we present the UVOT data without a red-leak correction.

The results of our UVOT analysis are displayed in Figure 2 and presented in Table 3.

To correct the KAIT and *Swift* photometry for small systematic differences due to different instrumental response functions, we apply *S*-corrections to put our optical photometry on the standard system following the method of Stritzinger et al. (2002). This procedure is done in addition to standard color-corrections which are appropriate for stellar SEDs, but can be inaccu-

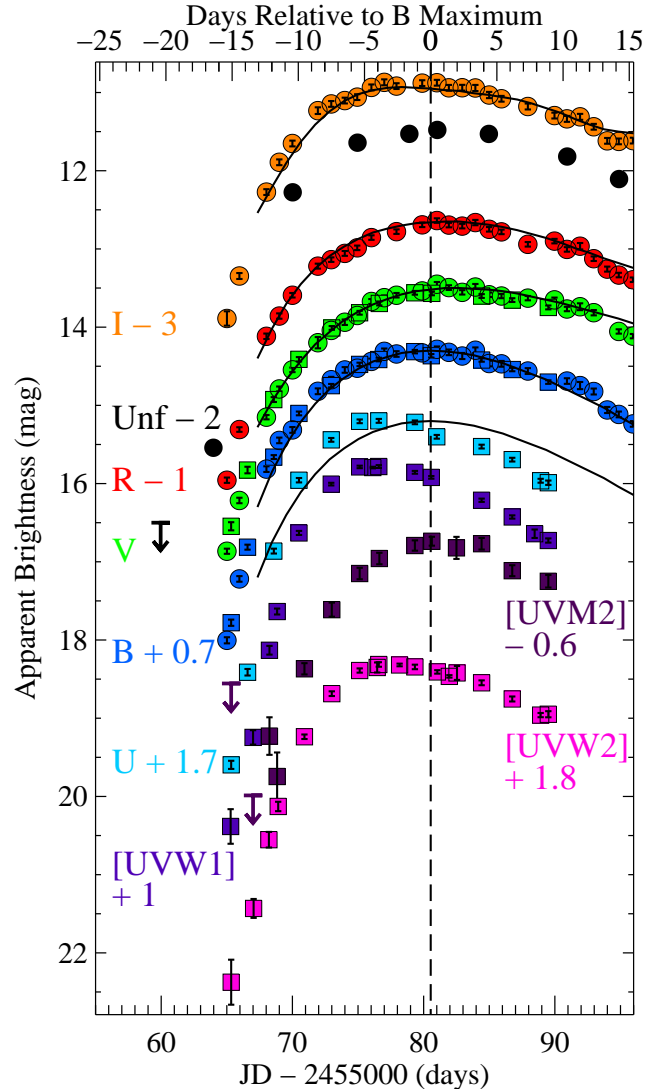


FIG. 2.— $[UVW2][UVM2][UVW1]UBVRI$ (fuchsia, dark purple, navy, cyan, blue, green, red, and orange, respectively; circles and squares correspond to KAIT and *Swift*/UVOT data, respectively) and unfiltered (black circles, with the label “Unf”) light curves of SN 2009ig. Our unfiltered magnitudes closely approximate the *R* band. The uncertainties for most data points are smaller than the plotted symbols. Also shown are comparison *UBVRI* template light curves of SN 2005cf (Wang et al. 2009b), stretched by a factor of 1.1.

rate for the SED of a SN. The instrumental response function includes the effects of the filter transmission, quantum efficiency of the detector, mirror reflectivity, and the atmospheric transmission in the case of ground based telescopes. The instrumental response functions for our KAIT photometry correspond to KAIT4 in Ganeshalingam et al. (2010). We calculate synthetic magnitudes for the SN using the Bessel transmission curves of Stritzinger et al. (2005) and the instrumental response functions using our optical spectral series for SN 2009ig. In instances where our spectra of SN 2009ig do not cover the *B*-band (e.g., around maximum light), we instead use spectra from the Hsiao et al. (2007) spectral series at the appropriate phase warped using a third-order spline to match the colors of the KAIT natural system photometry. The difference between the

TABLE 1
PHOTOMETRY OF SN 2009IG STANDARD STAR

ID	α (J2000)	δ (J2000)	$B(\sigma_B)$	N_B	$V(\sigma_V)$	N_V	$R(\sigma_R)$	N_R	$I(\sigma_I)$	N_I
1	02:37:58.65	-01:16:56.4	13.637 (004)	6	13.039 (003)	6	12.829 (007)	4	12.426 (015)	3

NOTE. — Photometry given in magnitudes with 1σ uncertainties (in mmags) presented in parentheses. N corresponds to the number of calibration images for each band.

TABLE 2
KAIT PHOTOMETRY AND S-CORRECTIONS FOR SN 2009IG

JD	B (mag)	S_B (mag)	V (mag)	S_V (mag)	R (mag)	S_R (mag)	I (mag)	S_I (mag)
2455065.01	17.304 (039)	-0.110	16.865 (033)	0.010	16.957 (034)	0.020	16.889 (092)	-0.020
2455065.96	16.519 (036)	-0.100	16.216 (035)	0.000	16.309 (029)	0.020	16.346 (038)	-0.020
2455068.02	15.115 (036)	-0.050	15.151 (028)	-0.010	15.117 (035)	0.010	15.273 (037)	-0.010
2455069.00	14.748 (036)	-0.040	14.790 (031)	-0.010	14.858 (034)	0.010	14.892 (037)	-0.010
2455070.00	14.614 (037)	-0.040	14.546 (029)	-0.010	14.592 (029)	0.010	14.652 (037)	-0.010
2455071.94	14.120 (037)	-0.030	14.199 (072)	-0.010	14.220 (032)	0.000	14.232 (043)	-0.010
2455072.96	13.972 (037)	-0.030	14.042 (028)	-0.010	14.137 (029)	0.010	14.146 (037)	-0.010
2455073.99	13.847 (036)	-0.030	13.937 (035)	-0.010	14.057 (031)	0.010	14.103 (037)	-0.010
2455074.94	13.825 (036)	-0.030	13.851 (028)	0.000	13.986 (029)	0.010	14.059 (037)	-0.010
2455076.02	13.738 (036)	-0.020	13.672 (031)	0.000	13.855 (029)	0.020	13.935 (038)	-0.020
2455077.00	13.609 (036)	-0.030	13.623 (028)	0.000	...	0.020	13.870 (038)	-0.020
2455077.93	13.643 (036)	-0.030	13.592 (029)	0.000	13.779 (029)	...	13.918 (037)	-0.020
2455079.89	13.629 (036)	-0.040	13.537 (028)	0.000	13.692 (029)	0.030	13.880 (037)	-0.020
2455081.01	13.583 (036)	-0.030	13.451 (028)	0.000	13.637 (029)	0.030	13.875 (037)	-0.030
2455081.92	13.622 (036)	-0.030	13.494 (030)	0.000	13.695 (029)	0.030	13.940 (037)	-0.030
2455082.94	13.669 (039)	-0.030	13.555 (028)	0.000	13.708 (029)	0.030	13.939 (037)	-0.030
2455083.94	13.595 (036)	-0.030	13.487 (039)	0.000	13.663 (034)	0.030	13.942 (039)	-0.030
2455084.99	13.765 (036)	-0.030	13.586 (029)	0.000	13.749 (029)	0.040	14.032 (040)	-0.030
2455085.93	13.769 (037)	-0.030	13.602 (028)	0.000	13.782 (029)	0.030	14.080 (037)	-0.030
2455087.94	13.861 (037)	-0.030	13.629 (028)	0.000	13.941 (029)	0.030	14.179 (038)	-0.040
2455089.97	13.651 (029)	-0.010	13.900 (029)	0.030	14.295 (037)	-0.040
2455090.92	13.989 (036)	-0.030	13.768 (028)	-0.010	14.006 (029)	0.020	14.337 (038)	-0.040
2455091.92	14.047 (046)	-0.040	13.739 (044)	-0.010	13.965 (041)	0.020	14.311 (038)	-0.050
2455092.96	14.123 (038)	-0.040	13.815 (034)	0.000	14.125 (029)	0.020	14.438 (037)	-0.050
2455093.99	14.359 (039)	-0.040	14.258 (032)	0.020	14.618 (037)	-0.050
2455094.87	14.416 (037)	-0.021	14.055 (028)	0.000	14.334 (029)	0.010	14.625 (037)	-0.050
2455095.95	14.537 (036)	-0.020	14.115 (028)	0.000	14.394 (029)	0.010	14.615 (037)	-0.050
2455097.02	14.639 (038)	-0.020	14.085 (030)	0.000	14.345 (029)	0.010	14.606 (037)	-0.050
2455097.90	14.776 (038)	-0.020	14.238 (028)	0.000	14.460 (029)	0.010	14.663 (037)	-0.050
2455098.93	14.885 (036)	-0.030	14.203 (028)	0.010	14.482 (029)	0.010	14.621 (037)	-0.060
2455099.94	15.000 (036)	-0.020	14.301 (029)	0.010	14.470 (029)	0.020	14.601 (037)	-0.050
2455100.93	15.113 (042)	-0.030	14.444 (031)	0.020	14.515 (037)	-0.050
2455101.98	15.145 (037)	-0.040	14.330 (028)	0.010	14.476 (029)	0.020	14.461 (040)	-0.050
2455102.96	15.175 (036)	-0.050	14.335 (028)	0.010	14.425 (029)	0.020	14.435 (037)	-0.040
2455104.96	15.381 (036)	-0.060	14.413 (028)	0.010	14.403 (029)	0.030	14.394 (037)	-0.030
2455106.87	15.591 (039)	-0.050	14.524 (029)	0.010	14.425 (029)	0.030	14.434 (037)	-0.020
2455112.91	16.076 (044)	-0.060	14.825 (029)	0.020	14.666 (030)	0.030
2455114.90	16.112 (037)	-0.060	14.928 (038)	0.020	14.781 (029)	0.020	14.430 (037)	-0.010
2455116.96	16.206 (091)	-0.060	15.104 (029)	0.010	14.916 (029)	0.020	14.544 (037)	-0.010
2455120.93	16.288 (036)	-0.080	15.292 (028)	0.010	15.066 (031)	0.020	14.754 (037)	0.000
2455123.89	16.480 (039)	-0.080	15.388 (028)	0.010	15.337 (029)	0.030	15.049 (037)	-0.010
2455126.91	16.418 (036)	-0.060	15.448 (043)	0.010	15.363 (030)	0.030	15.169 (037)	0.000
2455129.81	16.514 (036)	-0.050	15.636 (029)	0.010	15.532 (029)	0.020	15.325 (037)	0.000
2455132.86	16.619 (047)	-0.050	15.721 (031)	0.010	15.572 (029)	0.020	15.442 (038)	0.010
2455133.85	16.546 (040)	-0.040	15.704 (029)	0.000	15.544 (034)	0.020	15.509 (037)	0.020
2455139.91	16.716 (063)	-0.040	15.941 (044)	0.000	15.809 (088)	0.020	15.880 (061)	0.020
2455143.81	17.001 (148)	-0.050	16.088 (043)	0.000	15.935 (031)	0.020	15.973 (047)	0.010
2455148.89	16.792 (044)	-0.020	16.081 (038)	0.010	16.074 (029)	0.010	16.063 (037)	0.010
2455154.82	16.974 (037)	0.000	16.316 (029)	0.010	16.326 (029)	0.000	16.397 (038)	0.010
2455159.77	16.983 (036)	0.020	16.376 (029)	0.000	16.402 (029)	0.000	16.490 (040)	0.010
2455168.81	17.187 (045)	0.040	16.682 (033)	0.000	16.820 (038)	0.010
2455173.83	17.295 (037)	0.030	16.745 (030)	0.000	16.835 (030)	-0.010	16.981 (040)	0.010
2455182.76	17.286 (036)	0.060	16.994 (030)	0.000	17.066 (041)	-0.010	17.385 (127)	0.010
2455188.71	17.527 (036)	0.050	17.095 (033)	0.000	17.263 (031)	-0.010	17.509 (069)	0.010
2455196.79	17.589 (061)	0.060

NOTE. — Photometry given in magnitudes with 1σ (photometric and calibration) uncertainties (in mmags) presented in parentheses. The noted S -corrections have been applied to the photometry.

TABLE 3
Swift/UVOT PHOTOMETRY OF SN 2009IG

JD	Filter	Magnitude	<i>S</i> -Correction (mag)
2455065.33	[UVW2]	20.575 (288)	...
2455067.04	[UVW2]	19.632 (121)	...
2455068.21	[UVW2]	18.753 (100)	...
2455068.92	[UVW2]	18.328 (060)	...
2455070.92	[UVW2]	17.437 (029)	...
2455073.00	[UVW2]	16.886 (030)	...
2455075.13	[UVW2]	16.590 (027)	...
2455076.46	[UVW2]	16.551 (064)	...
2455076.58	[UVW2]	16.513 (029)	...
2455078.17	[UVW2]	16.519 (017)	...
2455079.33	[UVW2]	16.544 (029)	...
2455081.04	[UVW2]	16.608 (022)	...
2455081.96	[UVW2]	16.665 (016)	...
2455082.54	[UVW2]	16.621 (089)	...
2455084.42	[UVW2]	16.747 (031)	...
2455086.75	[UVW2]	16.954 (032)	...
2455088.92	[UVW2]	17.160 (027)	...
2455089.50	[UVW2]	17.149 (039)	...
2455098.96	[UVW2]	18.295 (071)	...
2455105.96	[UVW2]	18.761 (089)	...
2455107.88	[UVW2]	19.067 (113)	...
2455113.79	[UVW2]	19.199 (112)	...
2455116.88	[UVW2]	19.297 (122)	...
2455065.33	[UVM2]	> 19.156	...
2455067.00	[UVM2]	> 20.587	...
2455068.25	[UVM2]	19.828 (240)	...
2455068.83	[UVM2]	20.345 (307)	...
2455070.92	[UVM2]	18.968 (072)	...
2455073.00	[UVM2]	18.212 (090)	...
2455075.13	[UVM2]	17.750 (073)	...
2455076.63	[UVM2]	17.558 (073)	...
2455079.33	[UVM2]	17.392 (066)	...
2455080.63	[UVM2]	17.337 (057)	...
2455082.50	[UVM2]	17.422 (141)	...
2455084.42	[UVM2]	17.369 (074)	...
2455086.75	[UVM2]	17.714 (070)	...
2455089.50	[UVM2]	17.849 (080)	...
2455098.96	[UVM2]	18.912 (147)	...
2455105.96	[UVM2]	19.480 (203)	...
2455107.88	[UVM2]	19.578 (220)	...
2455113.79	[UVM2]	20.346 (326)	...
2455116.88	[UVM2]	> 20.100	...
2455065.29	[UVW1]	19.384 (221)	...
2455067.00	[UVW1]	18.245 (092)	...
2455068.25	[UVW1]	17.131 (056)	...
2455068.83	[UVW1]	16.636 (038)	...
2455070.50	[UVW1]	15.631 (026)	...
2455072.96	[UVW1]	15.007 (017)	...
2455075.13	[UVW1]	14.787 (016)	...
2455076.13	[UVW1]	14.795 (010)	...
2455076.58	[UVW1]	14.782 (018)	...
2455079.33	[UVW1]	14.856 (018)	...
2455080.58	[UVW1]	14.921 (017)	...
2455084.42	[UVW1]	15.213 (021)	...
2455086.75	[UVW1]	15.427 (021)	...
2455088.46	[UVW1]	15.641 (054)	...
2455089.50	[UVW1]	15.728 (027)	...
2455098.96	[UVW1]	16.846 (049)	...
2455101.83	[UVW1]	17.145 (073)	...
2455105.92	[UVW1]	17.609 (072)	...
2455107.88	[UVW1]	17.713 (081)	...
2455113.79	[UVW1]	18.035 (090)	...
2455116.88	[UVW1]	18.481 (123)	...

Bessel synthetic magnitude and the color-corrected instrumental synthetic magnitude is the *S*-correction (See Stritzinger et al. 2002; Wang et al. 2009b, for more details on computing *S*-corrections). We fit splines to the KAIT *B* and *V* data to estimate the KAIT magnitudes at the time of the *Swift* observations in these bands. The residuals of KAIT minus *Swift* photometry in the *B* (*V*) band have a mean and standard deviation of -0.01 mag

TABLE 4
Swift/UVOT PHOTOMETRY OF SN 2009IG (CONTINUED)

JD	Filter	Magnitude	<i>S</i> -Correction (mag)
2455065.33	<i>U</i>	17.896 (068)	...
2455066.58	<i>U</i>	16.712 (042)	...
2455068.58	<i>U</i>	15.163 (021)	...
2455070.50	<i>U</i>	14.257 (015)	...
2455072.96	<i>U</i>	13.741 (011)	...
2455075.13	<i>U</i>	13.504 (011)	...
2455076.58	<i>U</i>	13.498 (012)	...
2455079.33	<i>U</i>	13.517 (012)	...
2455081.00	<i>U</i>	13.702 (006)	...
2455084.42	<i>U</i>	13.827 (012)	...
2455086.75	<i>U</i>	13.994 (012)	...
2455088.92	<i>U</i>	14.264 (005)	...
2455089.50	<i>U</i>	14.289 (015)	...
2455098.96	<i>U</i>	15.385 (024)	...
2455065.33	<i>B</i>	17.079 (040)	-0.047
2455066.58	<i>B</i>	16.113 (032)	-0.031
2455068.58	<i>B</i>	14.961 (025)	-0.022
2455070.50	<i>B</i>	14.403 (024)	-0.011
2455072.96	<i>B</i>	14.048 (022)	-0.012
2455075.12	<i>B</i>	13.776 (022)	-0.008
2455076.58	<i>B</i>	13.714 (023)	-0.002
2455079.33	<i>B</i>	13.613 (022)	-0.003
2455080.58	<i>B</i>	13.666 (022)	-0.005
2455084.42	<i>B</i>	13.720 (022)	-0.005
2455086.75	<i>B</i>	13.842 (022)	-0.008
2455089.50	<i>B</i>	14.002 (023)	-0.010
2455098.96	<i>B</i>	14.845 (025)	-0.011
2455105.96	<i>B</i>	15.483 (028)	-0.024
2455107.88	<i>B</i>	15.626 (030)	-0.027
2455113.79	<i>B</i>	16.015 (030)	-0.039
2455116.88	<i>B</i>	16.188 (033)	-0.025
2455065.33	<i>V</i>	16.546 (052)	0.031
2455066.58	<i>V</i>	15.827 (042)	0.027
2455068.58	<i>V</i>	14.926 (031)	0.017
2455070.50	<i>V</i>	14.411 (028)	0.026
2455073.00	<i>V</i>	14.010 (024)	0.017
2455075.13	<i>V</i>	13.816 (024)	0.032
2455076.63	<i>V</i>	13.697 (025)	0.038
2455079.33	<i>V</i>	13.561 (024)	0.036
2455080.63	<i>V</i>	13.568 (024)	0.034
2455084.42	<i>V</i>	13.602 (024)	0.033
2455086.75	<i>V</i>	13.654 (024)	0.044
2455089.50	<i>V</i>	13.748 (025)	0.047
2455098.96	<i>V</i>	14.273 (028)	0.043
2455105.96	<i>V</i>	14.515 (029)	0.037
2455107.88	<i>V</i>	14.631 (030)	0.037
2455113.79	<i>V</i>	14.925 (031)	0.041
2455116.88	<i>V</i>	15.199 (034)	0.036

NOTE. — Photometry given in magnitudes with 1σ uncertainties (in mmags) presented in parentheses. The noted *S*-corrections have been applied to the photometry.

(-0.03 mag) and 0.07 mag (0.06 mag), respectively.

2.2. Optical Spectroscopy

We obtained low- and medium-resolution optical spectra of SN 2009ig with the Kast double spectrograph (Miller & Stone 1993) on the Shane 3 m telescope at Lick Observatory, the Low Resolution Spectrograph (LRS; Hill et al. 1998) on the Hobby-Eberly Telescope (HET) in queue mode (Shetrone et al. 2007), the Blue Channel spectrograph (Schmidt et al. 1989) on the 6.5 m MMT telescope, the Low Resolution Imaging Spectrometer (LRIS; Oke et al. 1995) on the 10 m Keck I telescope, and the DEep Imaging Multi-Object Spectrograph (DEIMOS; Faber et al. 2003) on the 10 m Keck II telescope. Spectra were typically made at low airmass and at the parallactic angle (Filippenko 1982). A log of our observations is given in Table 5.

TABLE 5
LOG OF OPTICAL SPECTRAL OBSERVATIONS

Phase ^a	UT Date	Telescope / Instrument	Exposure (s)	Observer ^b
-14.2	2009 Aug. 22.508	Lick/Kast	1800	MC
-14.1	2009 Aug. 22.628	Keck/LRIS	300	AS, HS
-14.1	2009 Aug. 22.635	Keck/DEIMOS	2 × 120, 2 × 60	ET, RB, RG
-13.3	2009 Aug. 23.428	HET/LRS	900	SO
-13.1	2009 Aug. 23.623	Keck/DEIMOS	4 × 300	ET, RB, RG
-12.2	2009 Aug. 24.518	Lick/Kast	900	VB
-12.1	2009 Aug. 24.638	Keck/DEIMOS	3 × 300	ET, RB, RG
-11.2	2009 Aug. 25.522	Lick/Kast	900	VB
-11.1	2009 Aug. 25.632	Keck/DEIMOS	300	ET, JK, RB
-10.3	2009 Aug. 26.495	MMT/Blue Channel	180	GW
-10.1	2009 Aug. 26.637	Keck/DEIMOS	3 × 300	ET, JK, RB
-9.3	2009 Aug. 27.490	MMT/Blue Channel	180	FV, LJ
-9.3	2009 Aug. 27.499	Lick/Kast	600	SBC, DP
-8.3	2009 Aug. 28.493	MMT/Blue Channel	180	FV, LJ
-8.2	2009 Aug. 28.530	Lick/Kast	1500	AM, JS, MK
-7.4	2009 Aug. 29.421	HET/LRS	450	SR
-7.3	2009 Aug. 29.495	MMT/Blue Channel	120	FV, LJ
-6.4	2009 Aug. 30.407	HET/LRS	450	SR
-6.3	2009 Aug. 30.440	MMT/Blue Channel	120	FV, LJ
-5.4	2009 Aug. 31.402	HET/LRS	550	JC
-5.3	2009 Aug. 31.480	MMT/Blue Channel	120	GW
-3.4	2009 Sep. 02.402	HET/LRS	450	JC
-2.3	2009 Sep. 03.490	HET/LRS	450	SO
-1.4	2009 Sep. 04.472	HET/LRS	450	SO
-0.4	2009 Sep. 05.404	HET/LRS	450	SO

^a Days since *B* maximum, 2009 Sep. 6.0 (JD 2,455,080.5).

^b AM = A. Morton, AS = A. Stockton, SBC = S. B. Cenko, DP = D. Poznanski, ET = E. Tollerud, FV = F. Vilas, GW = G. Williams, HS = H.-Y. Shih, JC = J. Caldwell, JK = J. Kalirai, JS = J. Silverman, LJ = L. Jiang, MC = M. Childress, MK = M. Kandrashoff, RB = R. Beaton, RG = R. Guhathakurta, SO = S. Odewahn, SR = S. Rostopchin, VB = V. Bennert

Standard CCD processing and spectrum extraction were accomplished with IRAF. The data were extracted using the optimal algorithm of Horne (1986). Low-order polynomial fits to calibration-lamp spectra were used to establish the wavelength scale, and small adjustments derived from night-sky lines in the object frames were applied. The DEIMOS data were reduced using a modified version of the DEEP2 data-reduction pipeline¹⁸, which bias corrects, flattens, rectifies, and sky subtracts the data (Foley et al. 2007). We employed our own IDL routines to flux calibrate the data and remove telluric lines using the well-exposed continua of the spectrophotometric standards (Wade & Horne 1988; Matheson et al. 2000; Foley et al. 2003). Our optical spectra are presented in Figure 3.

2.3. Ultraviolet Spectroscopy

SN 2009ig was observed with the UV grism on *Swift*/UVOT for eight pointings totaling 82608 s between 2009 August 23.7 and 2009 September 14.4. The UVOT grism has spectral resolution $R = 150$, and a wavelength accuracy of about 7 Å. The observations were obtained in “clocked” mode, which limits contamination by unrelated zero orders at wavelengths longer than ~ 3200 Å. The grism reduction software had several updates compared to that used by Bufano et al. (2009), including a wavelength equation that varied with detector position, an extraction slit that followed the small spectral curvature, and the use of a ninth-order polynomial to better follow the rapidly changing background. The gross spectrum was extracted using a slit of width 13 pixels, and

TABLE 6
LOG OF *Swift*/UVOT SPECTRAL OBSERVATIONS

Phase ^a	UT Date	Exposure (s) ^b
-13.0	2009 Aug. 23.72	5742
-12.0	2009 Aug. 24.72	6601
-11.1	2009 Aug. 25.66	1491
-9.2	2009 Aug. 27.57	13803
-4.2	2009 Sep. 1.65	5764
-2.1	2009 Sep. 3.70	13318
1.5	2009 Sep. 7.34	17775
8.5	2009 Sep. 14.43	19259

^a Days since *B* maximum, 2009 Sep. 6.0 (JD 2,455,080.5).

^b Exposure times are corrected for dead time.

the background was extracted within 11 pixels of the gross slit to minimize contamination by the galaxy nucleus. Due to an unfavorable roll angle, the background of the first two spectra was contaminated by a bright F star, but there was no obvious contamination of any other spectra. To reduce the contamination from the F star, background regions starting only 1 pixel from the SN were chosen for the first two spectra. The contamination is minimal, but there is still some slight oversubtraction of flux for these spectra. Details of our observations are presented in Table 6.

3. BASIC OBSERVATIONAL DATA

SN 2009ig is a very well-observed SN. Using our extensive photometry, we provide basic parameters for it. Fitting a polynomial through a restricted region of each

¹⁸ <http://astro.berkeley.edu/cooper/deep/spec2d/>.

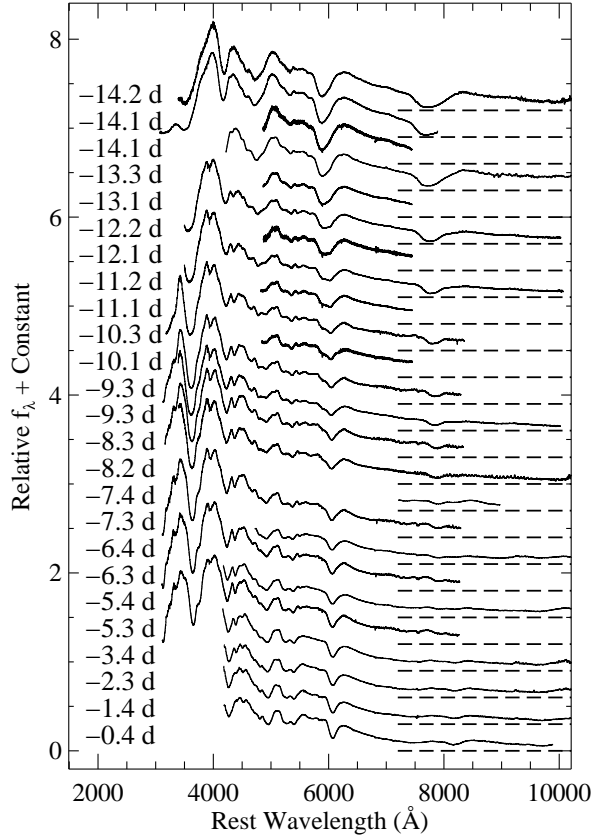


FIG. 3.— Optical spectra of SN 2009ig. The spectra are denoted by their phase relative to maximum brightness in the B band. The zero-flux level is indicated for each spectrum by a dashed line.

light curve, we determine the maximum-light characteristics presented in Table 7.

SN 2009ig peaked at $V = 13.52$ mag, making it one of the brightest SNe Ia of the last decade. The decline rate, $\Delta m_{15}(B) = 0.89$ mag, indicates that it was a slightly slower decliner than a nominal SN Ia with $\Delta m_{15} = 1.1$ mag. Using Milky Way reddening values (Schlegel et al. 1998) and the assumed distance modulus, but neglecting any potential host-galaxy reddening, we find that SN 2009ig had a peak absolute magnitude of $M_V = -19.19 \pm 0.40$ mag. Fitting the KAIT $BVRI$ light curves with MLCS2k2 (Jha et al. 2007), we find $\mu = 32.96 \pm 0.02$ mag (assuming $H_0 = 74 \text{ km s}^{-1} \text{ Mpc}^{-1}$), consistent with the Tully-Fisher measurement of $\mu = 32.6 \pm 0.4$ mag (Tully 1988).

The MLCS2k2 fit also finds a host-galaxy extinction of $A_V = 0.01 \pm 0.01$ mag, consistent with no host-galaxy reddening. Examination of the optical spectra shows that there is somewhat strong Na I D absorption (equivalent width 0.4 Å) at the redshift of the SN. However, this level of absorption is consistent with zero host-galaxy reddening as determined from large samples of SNe Ia (Blondin et al. 2009; Folatelli et al. 2010; Poznanski et al. 2011).

4. ULTRAVIOLET SPECTROSCOPY

Under our program to get *Swift* UV spectra of nearby SNe Ia (GI-5080130; PI Filippenko), we obtained eight low-resolution UV spectra of SN 2009ig. Six spectra were from before maximum brightness, a 38% increase in

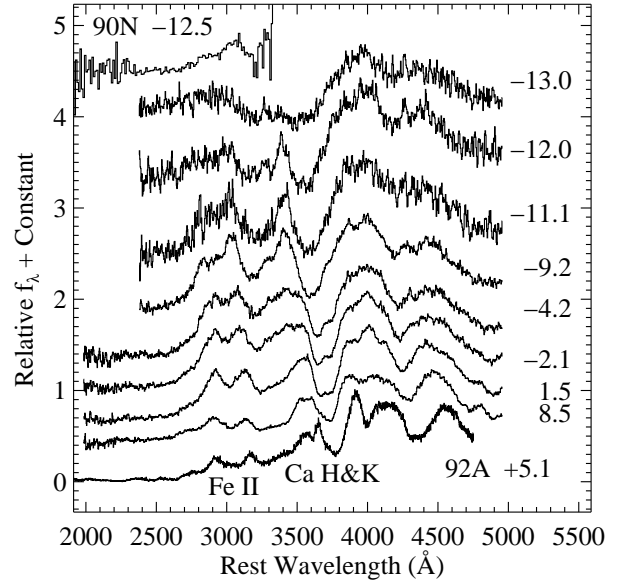


FIG. 4.— UV spectra of SN 2009ig. The spectra are denoted by their phase relative to maximum brightness in the B band. Also plotted are the previously earliest spectrum of a SN Ia, SN 1990N at $t = -12.5$ days (Leibundgut et al. 1991), and the earliest high-quality, true UV spectrum of a SN Ia, SN 1992A at $t = 5.1$ days (Kirshner et al. 1993).

the published premaximum UV spectra of SNe Ia. The first spectrum was taken -13.0 days before B maximum, making it the earliest UV spectrum ever obtained of a SN Ia. The SN was spectroscopically followed by *Swift* until 8.5 days after maximum brightness. The earliest spectrum shows a very broad absorption feature spanning $\sim 3000\text{--}4000$ Å; however, it separates into two distinct features (Co II and Ca H&K) only a day later. The UV continuum ($2500\text{--}3000$ Å) is high in the first spectrum, declining over the next 2–4 days, at which point it is relatively similar for all following epochs. The background region of the first spectrum was slightly contaminated by a nearby star (see Section 2.3), but this has the affect of reducing the continuum.

The absorption feature at ~ 3000 Å, attributed to Fe II $\lambda 3250$ (Branch & Venkatakrishna 1986), is possibly present at $t \leq -9.2$ days, although it is quite weak. Even at $t = -4.2$ days, it is not particularly strong. However, at $t = -2.1$ days, it has become rather strong, and by $t = 1.5$ days, it is very strong, similar to that of other SNe Ia (Foley et al. 2008).

The Fe II $\lambda 3250$ feature is the strongest one in the UV. Its velocity and pseudo-equivalent width (pEW) evolution have been measured for several objects by Foley et al. (2008), who found that the velocity evolution is similar for all objects, but the strength of the feature near maximum brightness correlates with light-curve shape. We present the velocity and pEW measurements for SN 2009ig relative to the Foley et al. (2008) sample in Figures 5 and 6, respectively. SN 2009ig appears to follow the previously established trends; its velocity is consistent with that of other SNe Ia, while its pEW is small, as expected given its relatively broad light curve.

Overall, the UV spectral evolution of SN 2009ig is

TABLE 7
PHOTOMETRIC INFORMATION FOR SN 2009ig

Filter	[UVW2]	[VM2]	[UVW1]	<i>U</i>	<i>B</i>	<i>V</i>	<i>R</i>	<i>I</i>
JD of max. −2,455,000	78.30 ± 0.05	81.30 ± 0.05	76.76 ± 0.05	76.57 ± 0.08	80.54 ± 0.04	82.17 ± 0.03	81.33 ± 0.29	78.26 ± 0.25
Mag at max.	16.50 ± 0.04	17.31 ± 0.14	14.75 ± 0.04	13.46 ± 0.01	13.66 ± 0.03	13.52 ± 0.02	13.64 ± 0.02	13.88 ± 0.03
Peak abs. mag	−16.30 ± 0.40	−15.55 ± 0.42	−18.02 ± 0.40	−19.32 ± 0.40	−19.08 ± 0.40	−19.19 ± 0.40	−19.05 ± 0.40	−18.78 ± 0.40
Δm_{15} (mag)	1.03 ± 0.03	1.49 ± 0.10	1.10 ± 0.03	0.95 ± 0.01	0.89 ± 0.02	0.58 ± 0.01	0.69 ± 0.01	0.63 ± 0.02

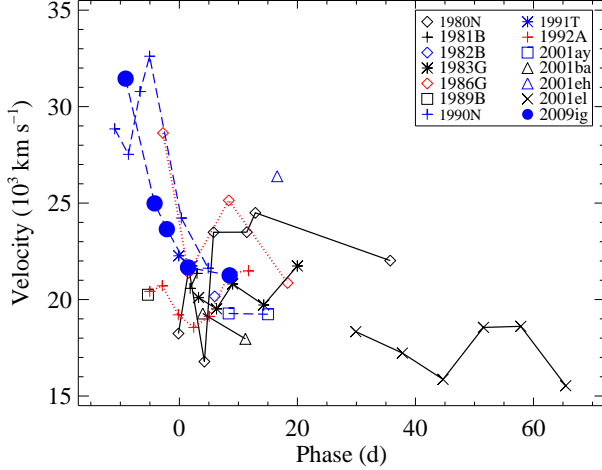


FIG. 5.— The blueshifted velocity of the minimum of the UV Fe II feature as a function of time for various SNe Ia assuming a rest-frame *gf*-weighted wavelength of 3250 Å. The normal, low, and high-luminosity (as defined by Foley et al. 2008) SNe Ia are shown in black, red, and blue (with solid, dotted, and dashed lines connecting points), respectively.

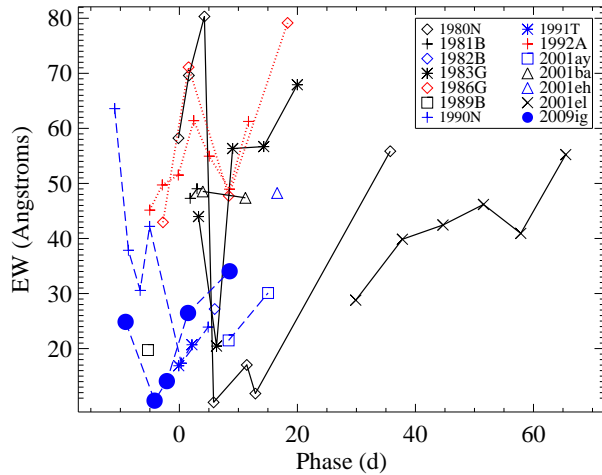


FIG. 6.— The pEW of the Fe II feature as a function of time for various SNe Ia. The normal, low, and high-luminosity (as defined by Foley et al. 2008) SNe Ia are shown in black, red, and blue (with solid, dotted, and dashed lines connecting points), respectively.

similar to that of other normal SNe Ia. Near maximum brightness, we measure a UV ratio ($\mathcal{R}_{UV} = f_{\lambda}(2770 \text{ Å})/f_{\lambda}(2900 \text{ Å})$; Foley et al. 2008) of 0.23, consistent with SN 2009ig having a relatively broad light curve. The shape of the SN Ia UV SED is determined by

several factors related to the progenitor and explosion. High-quality UV spectroscopy can disentangle these effects (Sauer et al. 2008). Unfortunately, the relatively low S/N data obtained at $\lambda < 2500 \text{ Å}$ precludes detailed modeling of the UV spectrum similar to what was done by Sauer et al. (2008).

5. EARLY-TIME PHOTOMETRY

5.1. Rise Time

The first detection of SN 2009ig was 16.4 days before *B* maximum, and therefore the rise time for SN 2009ig was ≥ 16.4 days. The last nondetection was 20.2 days before *B* maximum. However, extrapolating the light curve in any reasonable manner, the last nondetection is not sufficiently deep to be particularly constraining for the rise time. Nonetheless, SN 2009ig is one of the earliest ever detected SNe Ia.

Figure 7 shows the light curves of SN 2009ig, shifted such that the data represent the brightness below peak. Assuming that a SN is approximately a homologously expanding blackbody at early times, the luminosity of the SN should increase as a function of τ^2 , where τ is the time after explosion. This form assumes that there is negligible temperature evolution at early times, although Arnett (1982) showed that this form should be independent of temperature at sufficiently early times. Given the strong color evolution at early times (Section 5.2), this model may not apply to SN 2009ig.

Using a similar method to that of Riess et al. (1999), but without stretching the light curve, we fit the *B*-band data with $t < -10$ days to determine the rise time, t_r . The data are best fit with $t_r = 17.14 \pm 0.04$ days, where the uncertainty is only statistical. This fit is shown in Figure 7. However, there is a potential systematic difference in the measurement if the SN is not well described by a homologously expanding blackbody. Differences from this assumption should be larger at later times. If we examine only the first three KAIT data points (corresponding to 15.4, 14.5, and 12.4 days before *B* maximum), the best-fit rise time is $t_r = 17.11 \pm 0.07$ days, which is consistent with the other value. Nonetheless, we take the conservative approach of averaging the two values and using the larger uncertainty for our final measurement: $t_r = 17.13 \pm 0.07$ days. Our first detection at $t = -16.4$ days means that SN 2009ig was discovered ~ 17 hours after explosion. Measured rise times for SN 2009ig in all optical bands are consistently ~ 17 days. All photometric data indicate that SN 2009ig was discovered $\lesssim 1$ day after explosion.

Ganeshalingam et al. (2011) examined a large sample of low-redshift SN Ia light curves, focusing on their rise time. This sample included the *B* and *V* KAIT light curves of SN 2009ig that are presented here. However, the SN 2009ig light curves were not well fit by their tem-

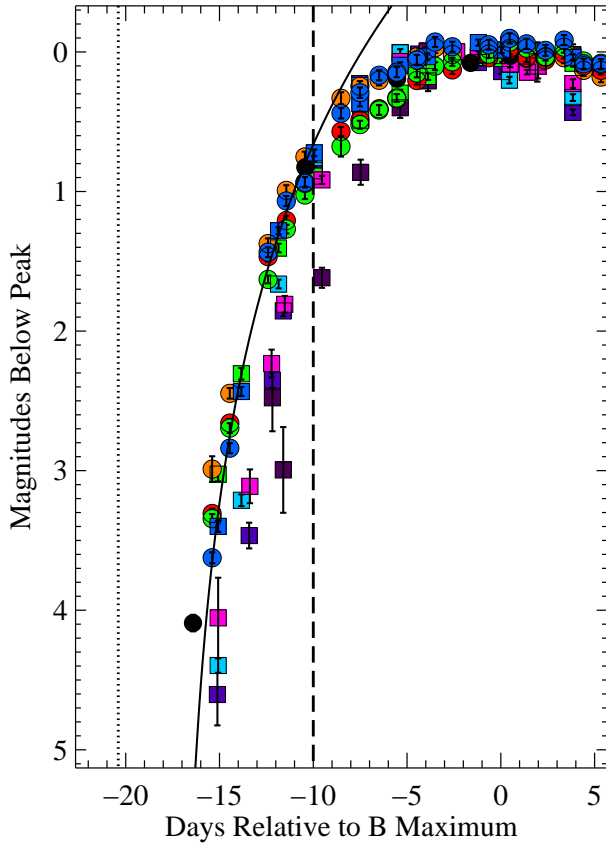


FIG. 7.— $[UVW2][UVM2][UVW1]UBVR$ (fuchsia, dark purple, navy, cyan, blue, green, red, and orange, respectively; circles and squares correspond to KAIT and *Swift*/UVOT data, respectively) and unfiltered (black circles, with the label “Unf”) light curves of SN 2009ig. The data have been shifted such that maximum brightness in each band corresponds to zero magnitude. The dotted line shows the time of the last nondetection, while the dashed line corresponds to $t = -10$ days. The solid curve represents the best-fit rise-time function for the B band with $t < -10$ days; the best-fit rise time is $t_r = 17.13$ days.

plate light curve, and SN 2009ig was rejected from their final analysis.

The rise time for SN 2009ig is relatively normal for a SN Ia. Hayden et al. (2010b) determined that the average SDSS SN Ia rise time is 17.38 ± 0.17 days (with a standard deviation in the sample of 1.8 days) in the B band. Strovink (2007) found an average rise time of 17.44 ± 0.39 days for a small sample of low-redshift SNe Ia with excellent premaximum light curves. SN 2009ig has high-velocity ejecta and a high velocity gradient for Si II $\lambda 6355$ (see § 6.1), and Pignata et al. (2008) suggested that high velocity gradient SNe Ia have shorter rise times than low velocity gradient SNe. Ganeshalingam et al. (2011) found that low-redshift high-velocity SNe Ia had a rise time of 16.63 ± 0.29 days. Observations of SN 2009ig support the trend that high-velocity SNe Ia tend to have shorter rise times in the B band.

Hayden et al. (2010b) and Ganeshalingam et al. (2011) note that their rise-time values are shorter than those found in previous studies (e.g., Riess et al. 1999, $t_r = 19.98 \pm 0.15$ days), but the differences are related to the adopted template light curve and a single-stretch

(rather than a two-stretch) method. Our method does not stretch the SN 2009ig light curves; we measure the true rise time of SN 2009ig.

SN 2009ig declined in the B band by 1.1 mag in 17.05 days; therefore, the difference between the rise and fall time for SN 2009ig is $t_r - t_f = 0.08$ days. This value is consistent with the majority of objects in the Hayden et al. (2010b) sample, but is slightly shorter than average. On the other hand, Ganeshalingam et al. (2011) found an average value of $t_r - t_f = 1.55 \pm 0.27$ days for high-velocity SNe Ia. The scatter is larger than the quoted uncertainty in the mean, but there are few SNe in their sample that have $t_r - t_f < 1$ day.

5.2. Color Curves

Examining the optical color curves shown in Figure 8, we see significant color evolution in $B - V$ for $t < -10$ days (this was also noted by Ganeshalingam et al. 2011). From $t = -15.2$ days to $t = -11.2$ days, $B - V$ decreased from 0.58 mag to 0.04 mag, a decline of $0.14 \text{ mag day}^{-1}$. The color changes in $V - R$ and $V - I$ are relatively small at early times ($\lesssim 0.2$ mag).

The UV color curves (Figure 9) also show very fast color evolution at early times. $[UVW2] - V$, $[UVM2] - V$, and $[UVW1] - V$ all become redder by ~ 1.5 mag from $t \approx -15$ days to $t \approx -5$ days. This is similar to the $U - V$ behavior, which is not unexpected given the effective wavelengths of the filters for a SN Ia SED. The color evolution is similar to the trends seen with a larger sample (Milne et al. 2010), but SN 2009ig extends these trends to much earlier phases.

Figures 8 and 9 compare the color curves of SN 2009ig to those of the commonly used SN Ia template light curves of Nugent et al. (2002) and Hsiao et al. (2007). After shifting to match the colors of SN 2009ig at maximum brightness, the templates reproduce the optical colors of SN 2009ig quite well for $t > -5$ days. The Nugent et al. (2002) and Hsiao et al. (2007) templates deviate from SN 2009ig for $t \lesssim -6$ and -9 days, respectively, in $B - V$. The $V - R$ colors appear to be more consistent out to the earliest observations of SN 2009ig, but there may be a significant deviation at $t \approx -10$ days. The Nugent et al. (2002) template matches the $V - I$ color of SN 2009ig at even its earliest epochs, but the Hsiao et al. (2007) template deviates significantly at $t \lesssim -12$ days.

There are no Nugent et al. (2002) template light curves for the UV bands, but we are able to synthesize light curves in the *Swift* bands from the Hsiao et al. (2007) template spectra using the in-orbit filter functions (Poole et al. 2008). The template matches SN 2009ig in $U - V$ and $[UVW1] - V$ after $t \approx -5$ days but is significantly bluer at earlier times, similar to $B - V$. The template light curves are generally very poor in $[UVW2] - V$ and $[UVM2] - V$ at all times, but are also bluer than the SN 2009ig data before maximum brightness (when normalizing to the color at maximum brightness). The long red tails for the UV filters should not directly affect the synthesized light curves if the filter definitions are correct. However, the tails can significantly affect the color curves depending on the reddening.

Since the Hsiao et al. (2007) (and to a lesser extent at this point, the Nugent et al. 2002) template is used for comparing data to a standard template and generating

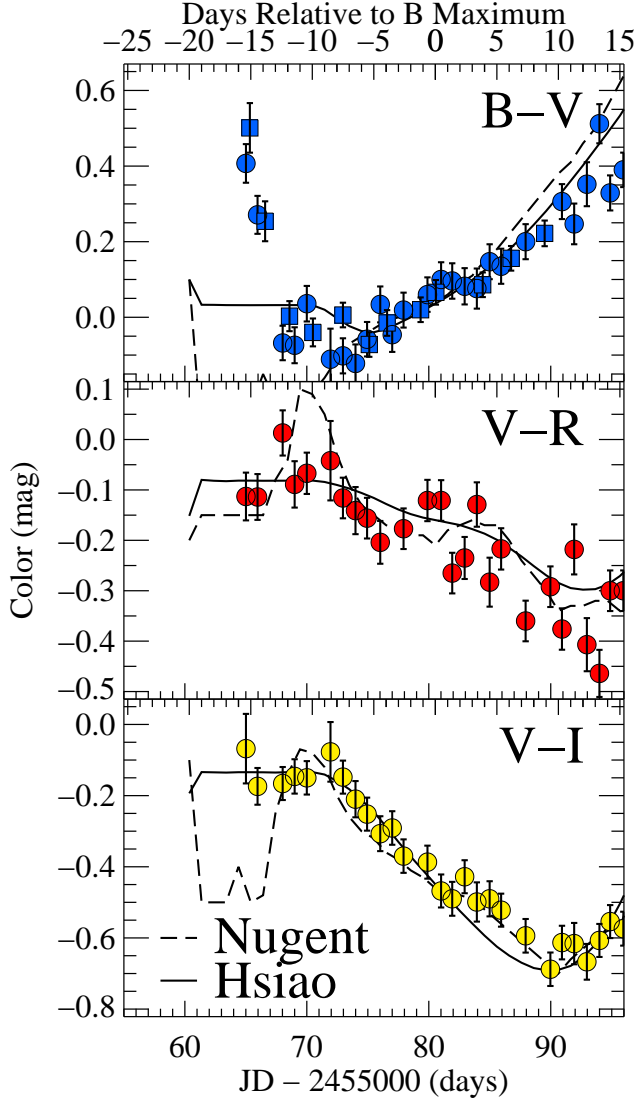


FIG. 8.— $B - V$, $V - R$, and $V - I$ color curves of SN 2009ig. All photometry has been corrected for the Milky Way reddening of $E(B - V) = 0.032$ mag (Schlegel et al. 1998). The solid and dashed lines represent the color curves of the Hsiao et al. (2007) and Nugent et al. (2002) template light curves, respectively, where each has been shifted to match SN 2009ig at maximum brightness.

K -corrections for high-redshift SN Ia light curves, its fidelity is important. Clearly, improvements can be made at early times. Nonetheless, the exact colors of the template are not important for K -corrections (since the template SED is warped to match the observed colors), but we show in Section 6.1 that there are significant differences between SN 2009ig and the Hsiao et al. (2007) template spectrum in the spectral features at early times. Interestingly, Hayden et al. (2010b) presents a K -corrected composite SDSS SN Ia $B - V$ color curve (their Figure 11) that has $B - V \approx 0 \pm 0.08$ mag for $t \leq -10$ days, which is significantly different from what is seen in SN 2009ig, but is consistent with the Hsiao et al. (2007) colors. Although SN 2009ig may be a significant outlier, it is likely that the $B - V$ color measured by Hayden et al. (2010b) was significantly affected by K -corrections which used the Hsiao et al. (2007) template. Similar to the above

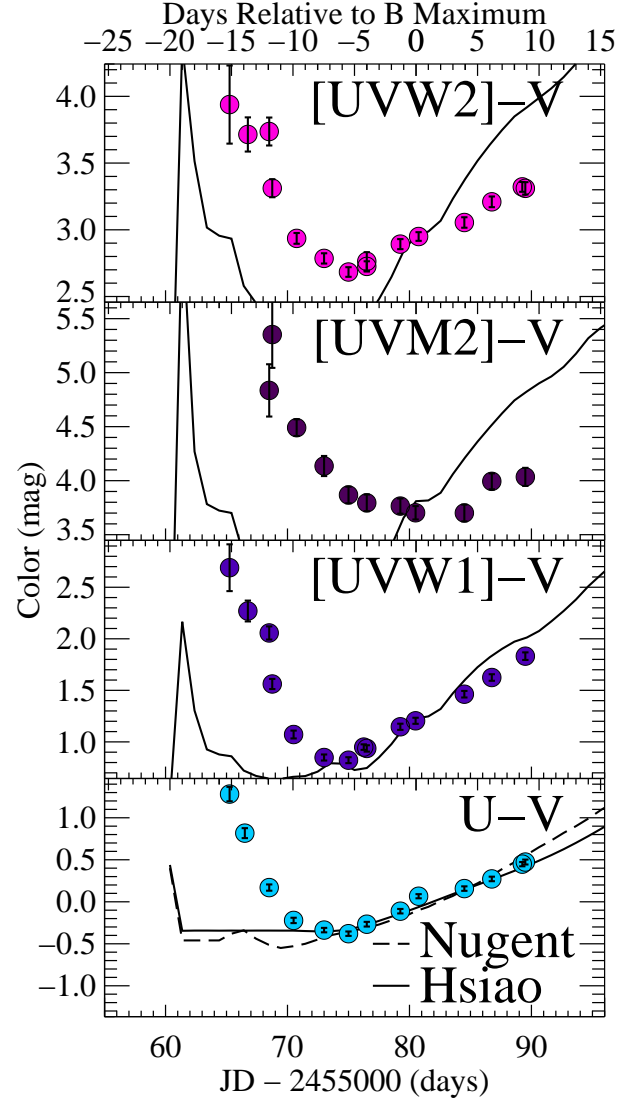


FIG. 9.— $[UVW2] - V$, $[UVM2] - V$, $[UVW1] - V$, and $U - V$ color curves of SN 2009ig (all obtained with *Swift*). All photometry has been corrected for the Milky Way reddening of $E(B - V) = 0.032$ mag (Schlegel et al. 1998) and the reddening corrections of Brown et al. (2010) for the *Swift* bands. The solid and dashed lines represent the color curves of the Hsiao et al. (2007) and Nugent et al. (2002) template light curves, respectively, where each has been shifted to match SN 2009ig at maximum brightness.

cases, light-curve fitters, which also use template light curves and SEDs, should consider these potential problems.

5.3. Emission from Interaction with a Companion Star

There is a simple observational prediction for a SN Ia that comes from a single-degenerate progenitor system where the companion star fills its Roche lobe: emission from the interaction of the SN ejecta with the companion star that can dominate over the light produced from radioactive decay at early times (Kasen 2010). The exact characteristics of the emission, particularly the peak luminosity and duration, depend on the progenitor system and viewing angle. Relative to the SN light curve, this emission should be brightest in the UV. The effect strongly depends on viewing angle, where signifi-

cant excess emission is observed when the viewing angle is aligned such that the companion star is between the WD and the observer, and essentially no additional emission is generated for viewing angles 180° from the WD-companion-observer configuration. For all companions explored by Kasen (2010) (a $1 M_\odot$ red giant, and 2 and $6 M_\odot$ main-sequence stars — all undergoing Roche-lobe overflow so that the radius of the companion is approximately half the separation distance), we would expect some excess emission in the B band at $\tau \approx 2$ days if we observed the SN from $\sim 10^\circ$ from the direction of the companion; the UV bands should display an even stronger signal.

In Figures 2 and 7, we see no indication of early excess emission in the optical bands. However, there is some indication of excess emission at early times in the UV. Because of their relatively low S/N, the $[UVM2]$ data are not particularly constraining. However, the $[UVW2]$ and $[UVW1]$ data suggest some excess emission. We caution that because of the long red tail in these bands, the apparent excess emission may be the result of optical color evolution.

A strong indication that there is no detected interaction is that the $B-V$ and UV colors of SN 2009ig at early times (our earliest measurement is ~ 0.7 day after explosion) are relatively red and get bluer until $t \approx -10$ days. This color evolution is not expected for the Kasen (2010) models.

To place further limits on excess emission at early times, the Kasen (2010) models are examined in more detail. The models produced are for the radioactively powered and interaction powered components combined. Since the Kasen (2010) models do not precisely reproduce the radioactively powered light curves, we have decided to examine the difference between the light curves from various viewing angles and the model light curve from a viewing angle farthest from the companion (167°). There may be excess emission from the interaction with the companion even in this model, so the difference between the models can be considered a lower limit on the expected emission for a given viewing angle.

Figure 10 shows the SN 2009ig light-curve data after subtracting an expanding fireball model. As explained above, this should be a reasonable model for the early-time behavior of a SN Ia. For this comparison, we fit the data with $t < -10$ days relative to B maximum, but ignored the first data point in each band. The strongest signal should be in the earliest data. This results in a measurement of the observed flux above that expected from modeling the additional data. If there is detectable excess flux in other observations, then this should be apparent as systematic residuals to the expanding fireball model.

Because of their numerical limitations, the Kasen (2010) models have significant scatter in their flux from one epoch to another, corresponding to ~ 0.2 mag for each band. This scatter must be included in any potential detection. We define our threshold as three times the geometric mean of the model scatter and the photometric uncertainty of the earliest data point in each band. This detection limit is marked as a dashed line in Figure 10.

The first V -band observation is consistent with the expanding fireball model. The first B -band observation is slightly brighter than expected from the expanding fire-

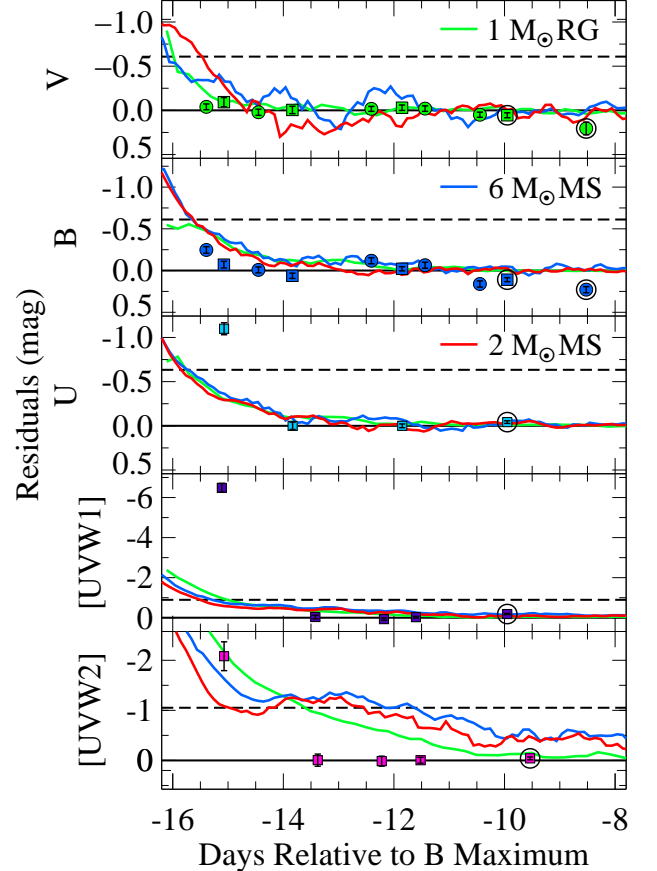


FIG. 10.— SN 2009ig $[UVW2][UVW1]UBV$ photometry (bottom to top panels) with an expanding fireball model subtracted. The expanding fireball model was fit to the data at $-15 < t < -10$ days relative to B maximum, which excludes the first one or two data points. The circled points are at $t > -10$ days and are not included in the fit. The green, blue, and red curves correspond to excess emission in the $1 M_\odot$ red-giant, $6 M_\odot$ main-sequence, and $2 M_\odot$ main-sequence companion Kasen (2010) models at viewing angles of 151° , 109° , and 68° , respectively. Specifically, these curves are an indication of the emission from the interaction only. These lines correspond to the largest viewing angle (relative to the companion star) consistent with B -band observations of SN 2009ig (i.e., are below the threshold at the time of the earliest observation). The dashed black line represents the threshold above which a band has excess emission.

ball model, but is not above our threshold. The first U -band measurement is significantly above our threshold, but only two data points were used to constrain the model. Both the $[UVW1]$ and $[UVW2]$ bands show significant excess in their first observations relative to the expanding fireball model. However, the models were fit with only three data points in each of these bands, so the fits may be biased. Nonetheless, this trend of excess flux in the UV bands is similar to what was seen in Figures 2 and 7. Furthermore, all bands bluer than V have excess flux in their first data point and the data slightly after $t = -10$ days are consistent with the model, making an excess more likely.

Using the Kasen (2010) model SEDs, we were able to construct residual light curves in each of our bands. Using the B threshold, we can place a limit on the possible viewing angle for the three progenitors considered. The $1 M_\odot$ red-giant, $6 M_\odot$ main-sequence, and $2 M_\odot$

main-sequence models with viewing angles (relative to the companion star) greater than 151° , 109° , and 68° , respectively, are consistent with this measurement (i.e., they have excess flux below the threshold at the time of the earliest B -band observation). Given the distribution of possible viewing angles, these values corresponds to $<6\%$, 34% , and 69% of the random viewing angles. Despite being formally inconsistent with a simple expanding fireball model, the $[UVW2]$ band is consistent with the Kasen (2010) models for the large angle considered above. The excess emission in the U and $[UVW1]$ bands is also in excess of these models/angles. In fact, the $[UVW1]$ data are inconsistent with all models/angles investigated by Kasen (2010).

The excess flux seen in the bluer bands appears to be real. Supporting this view are that the difference from the expanding fireball model is always an excess, data just after the phase range we use to fit the model are consistent with the model, there appears to be a visual excess in the bluest bands, and including the first data point in a fireball fit significantly increases the χ^2 per degree of freedom. However, the disagreement with the models in the various bands suggests that the simple Kasen (2010) model is not responsible for this excess. Instead, considering that the colors become bluer with time (the opposite of predictions) and the long tail of the UV filters, we suggest that the excess seen in the UV light curves is the result of optical (and perhaps UV) color evolution. If there is significant color evolution because of either changes to spectral features or the temperature, then the expanding fireball model may not be sufficient for modeling the early-time light curve.

Using samples of ~ 100 SNe Ia from SDSS and SNLS, respectively, Hayden et al. (2010a) and Bianco et al. (2011) produced K -corrected composite rest-frame B -band light curves. The ensemble of light curves did not show any deviation from a standard rise, indicating that red-giant progenitor systems must be a small fraction (if there is any contribution at all) of the SN Ia progenitor systems. Ganeshalingam et al. (2011) examined 61 well-sampled low-redshift SN Ia light curves, finding no signs of interaction under simple assumptions; however, relaxing these assumptions, they found large systematic trends in the data, precluding any definitive conclusions. Unlike previous work that focused on the statistical treatment of large samples, we have concentrated on a single well-observed SN, which can reduce some potential systematic biases. Nevertheless, the SN 2009ig data provide additional concern when making simple assumptions about the early-time light curves of SNe Ia.

6. OPTICAL SPECTROSCOPY

6.1. Early-Time Spectroscopy

In Figure 11, we show a detailed comparison of a subset of our earliest spectra. In the first panel, we compare spectra obtained -14.2 and -13.3 days relative to B maximum. Although these spectra are separated by only 1 day, there are some differences, particularly in the shape of the Ca II near-infrared (NIR) triplet. The second panel adds the spectrum at -12.2 days relative to B maximum. This spectrum is significantly different from that taken only two days earlier. In particular, the Ca II NIR triplet and the Si II $\lambda 6355$ features have very different shapes. The Si II $\lambda 6355$ feature has a flatter

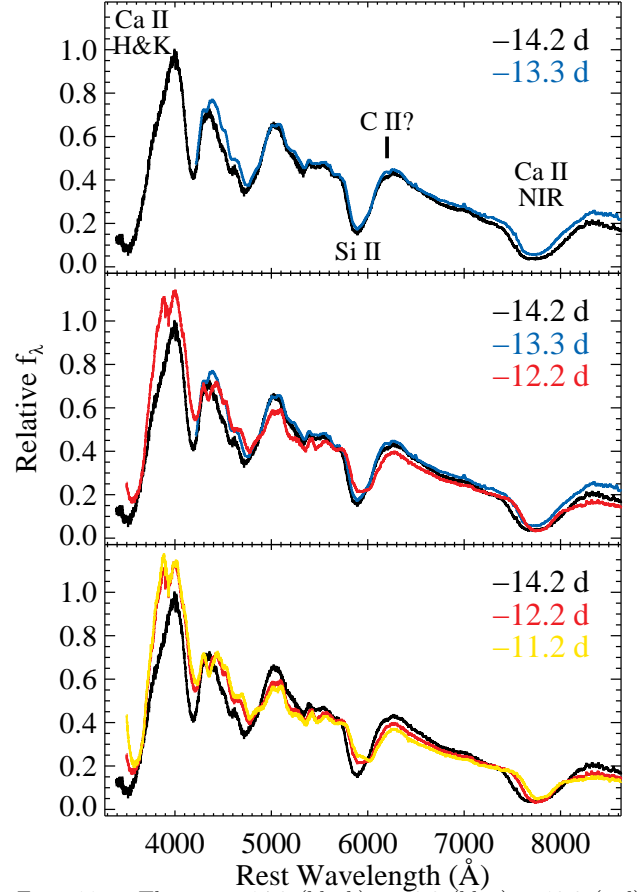


FIG. 11.— The $t = -14.2$ (black), -13.3 (blue), -12.2 (red), and -11.2 days (yellow) spectra of SN 2009ig. Features discussed in the text are labeled.

bottom and is much weaker at $t = -12.2$ days. The velocity of these features (as well as others, including Ca H&K) is significantly lower in the later spectrum. The continuum is also different, with the later spectrum being bluer, similar to what is seen in the $B - V$ color (Figure 8). The red wing of Ca H&K in the $t = -14.2$ days spectrum is non-Gaussian, with a change in the slope at ~ 3800 Å. The Si II $\lambda 4130$ feature is not distinct in the earliest spectrum. By $t = -12.2$ days, this feature is clear. We speculate that at earlier times, this feature is at higher velocity and simply blends with Ca H&K, causing the peculiar red wing of Ca H&K; however, it is possible that ionization effects suppress this feature at early times. The last panel of Figure 11 adds the $t = -11.2$ days spectrum. This spectrum is very similar to the $t = -12.2$ days spectrum in feature strength and continuum shape, but there is a noticeable difference in the velocities of the various features.

Parrent et al. (2011) analyzed two of the spectra presented here and attributed a small depression at ~ 6200 Å to C II $\lambda 6580$. Although we do not provide a detailed analysis of this feature, at ~ 6200 Å, we note that it is present in all of our first 6 spectra corresponding to $t \leq -12.2$ days. Those spectra were obtained with 4 separate telescope/instrument configurations, so we believe that it is a real feature. It is also present in our $t = -11.1$ days spectrum, but we do not have definitive detections for our $t = -12.1$ or -11.2 days spectra,

though this is possibly the result of those spectra having a relatively low S/N. We do not detect this feature in any later epochs, giving additional credibility to it being real. If this feature is C II $\lambda 6580$, it would correspond to a velocity of about $-17,000 \text{ km s}^{-1}$, making it much lower velocity than the velocity inferred from the minimum of Si II at the same epoch (about $-23,000 \text{ km s}^{-1}$), but may be consistent with an extrapolation of the lower-velocity Si II component extrapolated to the earliest epochs (see Section 6.2). If C II is detected, this would be the first detection of it in a high-velocity SN Ia.

The spectra of SN 2009ig change dramatically until about 12 days before maximum brightness. After this time, the general spectral features and shape stay relatively constant until after maximum brightness. This epoch also approximately corresponds to the time when the SN $B - V$ color evolution slows down (Section 5.2).

In Section 5.2, we showed that the early-time color evolution of SN 2009ig was poorly matched by the color evolution of the Hsiao et al. (2007) template spectra. However, that comparison is not apt for K -corrections and some other applications since it neglected to warp the template spectra to match the observed colors of SN 2009ig. Without warping, the Hsiao et al. (2007) template spectrum has different broad-band colors than SN 2009ig. We fit a spline to the ratio of the broad-band integrated fluxes of the template and SN spectra. The template spectrum is divided by the spline to warp the template spectrum to have the same $UBVRI$ magnitudes of the combined UV/optical SN 2009ig spectrum. In the top panel of Figure 12, we show the $t = -13.0$ days *Swift* UV spectrum, the $t = -14.2$ days optical spectrum, and the $t = -14$ days $UBVRI$ color-warped Hsiao et al. (2007) template spectrum. There are several differences between the SN 2009ig and Hsiao et al. (2007) spectra. In particular, the Hsiao et al. (2007) spectrum has weaker, lower-velocity features and significant deviations for $\lambda < 4000 \text{ \AA}$.

The bottom panel of Figure 12 displays the $t = -4.2$ days *Swift* UV spectrum, the $t = -5.8$ days optical spectra, and the $t = -5$ days $UBVRI$ color-warped Hsiao et al. (2007) template spectrum. At this phase, the Hsiao et al. (2007) template spectrum is a much better match to SN 2009ig; there are still some differences in the UV, particularly the feature at 2900 \AA and the continuum for $\lambda < 2600 \text{ \AA}$, but the match is significantly better than for the $t = -14$ days spectrum. Clearly, additional early-time data are necessary to improve the fidelity of template spectra and light curves. Use of the current template spectra will provide significantly discrepant K -corrections, even after 5-band color warping.

6.2. Si II $\lambda 6355$

While the overall shape of the spectrum of SN 2009ig shows most of its evolution during the first few days after explosion, individual spectral features continue to evolve for several more days. An example of this is the strong Si II $\lambda 6355$ line. Using the method outlined by Foley et al. (2011, and references therein), we determined the wavelength of maximum absorption for this feature; we present a characteristic velocity of the line in Figure 13.

SN 2009ig displays the highest-velocity Si II $\lambda 6355$ ever published, with the earliest spectra having

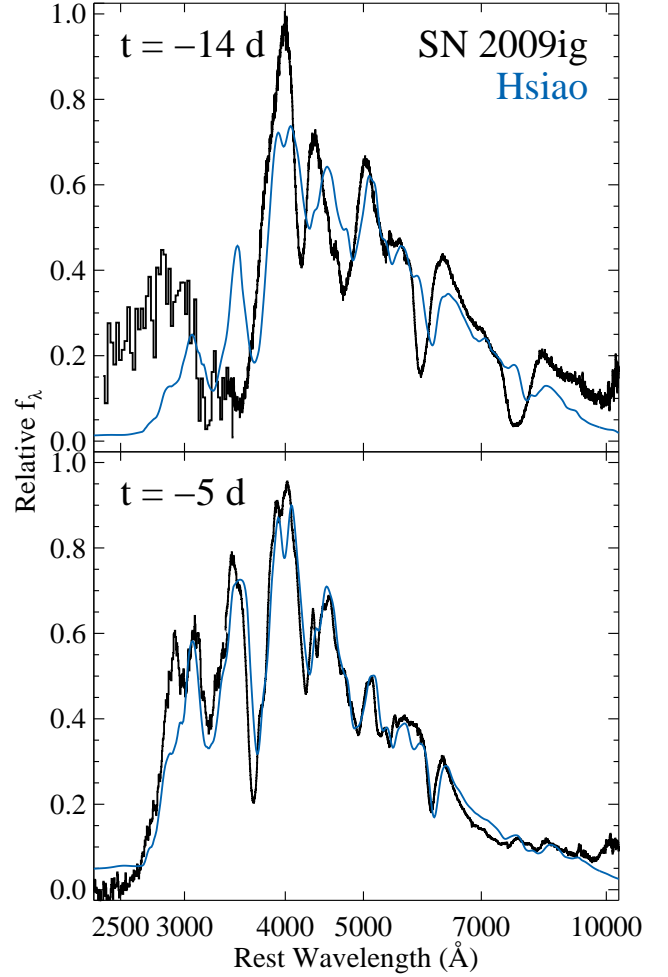


FIG. 12.— The $t = -13.0$ days *Swift* UV and $t = -14.2$ days optical spectra (top panel) and the $t = -4.2$ days *Swift* UV and $t = -5.8$ days optical spectra (bottom panel) of SN 2009ig (black curves). The blue curves are the $t = -14$ days and $t = -5$ days $UBVRI$ color-warped Hsiao et al. (2007) template spectra (top and bottom panels, respectively).

$v = -23,000 \text{ km s}^{-1}$ at $t = -14.2$ days, significantly faster than the fastest measurements of SN 2006X ($-20,700 \text{ km s}^{-1}$ on $t = -11.6$ days; Quimby et al. 2006) and SN 2003W ($-21,000 \text{ km s}^{-1}$ on $t = -11.2$ days; Foley et al. 2011). Navasardyan et al. (2009) reported an even higher velocity of $-24,500 \text{ km s}^{-1}$ for SN 2009ig on $t = -15.6$ days. For our first spectrum, the blue wing of Si II $\lambda 6355$ extends to at least 5720 \AA , corresponding to $v = -31,400 \text{ km s}^{-1}$ or $>0.1c$.

The velocity of the Si II $\lambda 6355$ feature evolves very quickly, decreasing by 5700 km s^{-1} in only 1.9 days. After this dramatic change, the velocity evolution appears to be linear in time, similar to that of most SNe Ia (Foley et al. 2011; Silverman et al., in prep.). The velocity near maximum brightness is about $-13,500 \text{ km s}^{-1}$, which is faster than $\sim 85\%$ of all SNe Ia with $1 \leq \Delta m_{15}(B) \leq 1.5 \text{ mag}$ and faster than $\sim 85\%$ of all SNe Ia with $\Delta m_{15}(B) \leq 1 \text{ mag}$ (Foley et al. 2011).

Further examination of the Si II $\lambda 6355$ feature demonstrates that the velocity evolution at early times is the

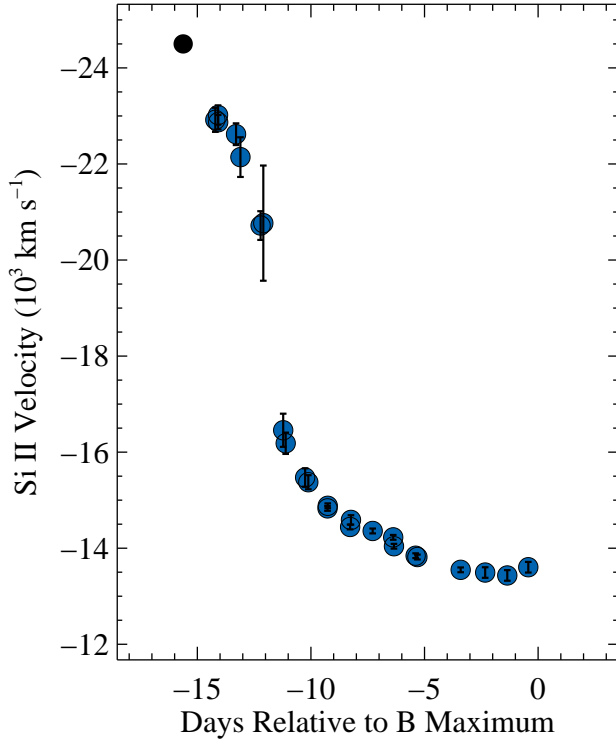


FIG. 13.— Velocity evolution of the Si II $\lambda 6355$ feature for SN 2009ig. The blue points come from our spectra. The black point was reported by Navasardyan et al. (2009).

result of multiple components. This is best displayed in Figure 14, which shows the Si II $\lambda 6355$ feature from spectra that occur before, during, and after this velocity change. At $t = -13.1$ days, there is some indication of two components, with the blue component dominating the profile. The relative strength quickly shifts; the components have similar strength at $t = -12.2$ days, but the red component is dominant by $t = -11.2$ days. This evolution continues to the point where the blue component is barely visible at $t = -9.3$ days. Further examination and discussion of the velocity evolution and line shapes of various features in the SN 2009ig spectra will be given by Marion et al. (in prep.).

7. DISCUSSION & CONCLUSIONS

SN 2009ig was discovered ~ 17 hours after explosion, relatively bright at peak ($V = 13.5$ mag), and well positioned for detailed monitoring. We obtained densely sampled UV/optical light curves, an unparalleled UV spectral sequence, and an excellent, almost nightly optical spectral sequence from discovery through maximum brightness. Here we have focused on the early-time properties of this SN, as well as on its unique UV spectral sequence.

SN 2009ig is a relatively normal SN Ia, although it is a slightly slow decliner ($\Delta m_{15}(B) = 0.89$ mag) and has relatively fast ejecta at maximum brightness ($v_{\text{Si II}}^0 \approx -13,500 \text{ km s}^{-1}$). We find that the rise time in the B band is 17.13 days, similar to that of other high-velocity SNe Ia. The UV spectral features are similar to those of other SNe Ia. Our observations, particularly the UV spectra and the early-time photometry and spectroscopy,

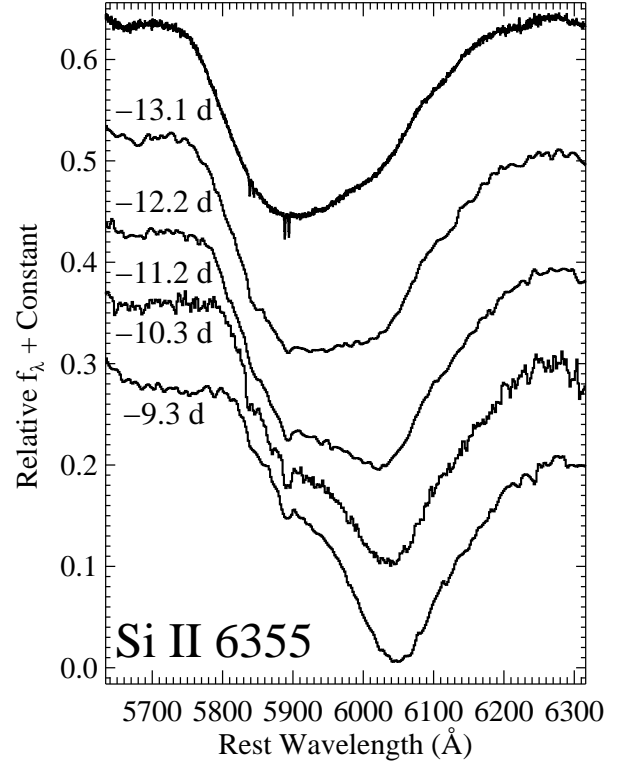


FIG. 14.— Spectra of SN 2009ig near the Si II $\lambda 6355$ feature. Phases are denoted for each spectrum.

greatly expand the existing data at these wavelengths and phases.

Despite being a relatively normal SN Ia, early-time observations deviate from template light curves and spectra: SN 2009ig is redder than the templates. Even after color warping an early-time template spectrum to match a spectrum of SN 2009ig at a similar phase, SN 2009ig has significantly broader, deeper, and higher-velocity spectral features than the template. The template also does a poor job at matching both the spectral features and the continuum at $\lambda < 4000 \text{ Å}$. Distance estimates that rely on K -corrections and/or early-time data from templates could be biased, directly impacting cosmological measurements. Studies that rely on early-time K -corrected data, such as measuring the rise time (Aldering et al. 2000; Conley et al. 2006; Hayden et al. 2010b) and interaction with a binary companion (Hayden et al. 2010a; Bianco et al. 2011) of high-redshift SNe Ia, may be biased by these differences. Low-redshift studies should be minimally affected. An examination of the early-time light curve of SN 2009ig shows excess emission relative to a simple expanding fireball model ($L \propto \tau^2$) in the UV bands. Although this behavior is expected if there is interaction between the SN and a binary companion, other predictions of the model (in particular, colors becoming redder) are not seen. It is therefore unlikely that we detect any interaction in the case of SN 2009ig.

SN 2009ig displays two velocity components in the Si II $\lambda 6355$ feature, with the higher-velocity component indicating the highest-velocity SN Ia ejecta ever observed. The relative strength of the components changes dra-

matically from $t = -13$ days to $t = -9$ days, and one would not infer the presence of a high-velocity feature from spectroscopy after $t = -9$ days. Since there are few available spectra of SNe Ia at such early epochs, high-velocity Si II $\lambda 6355$ may be ubiquitous or at least very common, like high-velocity Ca II features (Mazzali et al. 2005).

In the age of giant synoptic surveys including that of the Large Synoptic Survey Telescope, SNe similar to SN 2009ig will still be rare. Detailed studies of SNe that are as nearby, bright, well positioned, and found as soon after explosion as SN 2009ig have the potential to provide as much or more information for constraining progenitor and explosion models than large samples of more distant SNe.

Facilities: HET(LRS), Lick:KAIT, Lick:Shane(Kast), Keck:I(LRIS), Keck:II(DEIMOS), MMT(Blue Channel), Swift(UVOT)

R.J.F. is supported by a Clay Fellowship. We thank the anonymous referee for informed comments and suggestions. We thank D. Kasen for useful discussions. We are grateful to the staffs at the Lick, Keck, HET, and MMT Observatories for their dedicated services. J. Bullock, J. Caldwell, M. Kandrashoff, A. Morton, P. Nugent, S. Odewahn, D. Poznanski, S. Rostopchin, H.-Y. Shih, F. Vilas, and G. Williams helped obtain some of the data presented here; we also thank J. Lee and D. Tytler for attempting to obtain data. *Swift* spectroscopic observations were performed under program GI-5080130; we are very grateful to N. Gehrels and the *Swift* team for executing the program quickly. Super-

nova research at Harvard is supported by NSF grant AST-0907903. A.V.F.'s supernova group at U.C. Berkeley is supported by NASA/*Swift* grants NNX09AG54G and NNX10AF52G, NSF grant AST-0908886, Gary and Cynthia Bengier, the Richard and Rhoda Goldman Fund, and the TABASGO Foundation. J.V. received support from Hungarian OTKA Grant K76816, NSF Grant AST-0707769, and Texas Advanced Research Project grant ARP-0094.

Some of the data presented herein were obtained at the W. M. Keck Observatory, which is operated as a scientific partnership among the California Institute of Technology, the University of California, and NASA; the observatory was made possible by the generous financial support of the W. M. Keck Foundation. The Hobby-Eberly Telescope (HET) is a joint project of the University of Texas at Austin, the Pennsylvania State University, Stanford University, Ludwig-Maximilians-Universität München, and Georg-August-Universität Göttingen. The HET is named in honor of its principal benefactors, William P. Hobby and Robert E. Eberly. We acknowledge the use of public data from the *Swift* data archive. KAIT was constructed and supported by donations from Sun Microsystems, Inc., the Hewlett-Packard Company, Auto-Scope Corporation, Lick Observatory, the NSF, the University of California, the Sylvia & Jim Katzman Foundation, and the TABASGO Foundation. This research has made use of the NASA/IPAC Extragalactic Database (NED), which is operated by the Jet Propulsion Laboratory, California Institute of Technology, under contract with NASA.

REFERENCES

- Alard, C. 2000, *A&AS*, 144, 363
 Aldering, G., Knop, R., & Nugent, P. 2000, *AJ*, 119, 2110
 Amanullah, R., et al. 2010, *ApJ*, 716, 712
 Arnett, W. D. 1982, *ApJ*, 253, 785
 Bianco, F. B., et al. 2011, *ArXiv e-prints*, 1106.4008
 Blondin, S., Prieto, J. L., Patat, F., Challis, P., Hicken, M., Kirshner, R. P., Matheson, T., & Modjaz, M. 2009, *ApJ*, 693, 207
 Branch, D., & Venkatakrishna, K. L. 1986, *ApJ*, 306, L21
 Brown, P. J., et al. 2010, *ApJ*, 721, 1608
 Bufano, F., et al. 2009, *ApJ*, 700, 1456
 Burrows, D. N., et al. 2005, *Space Science Reviews*, 120, 165
 Colgate, S. A., & McKee, C. 1969, *ApJ*, 157, 623
 Conley, A., et al. 2011, *ApJS*, 192, 1
 ——. 2006, *AJ*, 132, 1707
 Cooke, J., et al. 2011, *ApJ*, 727, L35+
 Faber, S. M., et al. 2003, in *Instrument Design and Performance for Optical/Infrared Ground-based Telescopes*. Edited by Iye, Masanori; Moorwood, Alan F. M. *Proceedings of the SPIE*, Volume 4841, pp. 1657-1669 (2003)., ed. M. Iye & A. F. M. Moorwood, 1657-1669
 Filippenko, A. V. 1982, *PASP*, 94, 715
 Filippenko, A. V., Li, W. D., Treffers, R. R., & Modjaz, M. 2001, in *ASP Conf. Ser. 246: IAU Colloq. 183: Small Telescope Astronomy on Global Scales*, ed. B. Paczynski, W.-P. Chen, & C. Lemme, 121-+
 Folatelli, G., et al. 2010, *AJ*, 139, 120
 Foley, R. J., et al. 2009, *AJ*, 138, 376
 Foley, R. J., Filippenko, A. V., & Jha, S. W. 2008, *ApJ*, 686, 117
 Foley, R. J., & Kasen, D. 2011, *ApJ*, 729, 55
 Foley, R. J., Narayan, G., Challis, P. J., Filippenko, A. V., Kirshner, R. P., Silverman, J. M., & Steele, T. N. 2010, *ApJ*, 708, 1748
 Foley, R. J., et al. 2003, *PASP*, 115, 1220
 Foley, R. J., Sanders, N. E., & Kirshner, R. P. 2011, *ArXiv e-prints*, 1107.3555
 Foley, R. J., Smith, N., Ganeshalingam, M., Li, W., Chornock, R., & Filippenko, A. V. 2007, *ApJ*, 657, L105
 Ganeshalingam, M., Li, W., & Filippenko, A. V. 2011, *ArXiv e-prints*, 1107.2404
 Ganeshalingam, M., et al. 2010, *ApJS*, 190, 418
 Gehrels, N., et al. 2004, *ApJ*, 611, 1005
 Hamuy, M., et al. 2003, *Nature*, 424, 651
 Hayden, B. T., et al. 2010a, *ApJ*, 722, 1691
 ——. 2010b, *ApJ*, 712, 350
 Hicken, M., Wood-Vasey, W. M., Blondin, S., Challis, P., Jha, S., Kelly, P. L., Rest, A., & Kirshner, R. P. 2009, *ApJ*, 700, 1097
 Hill, G. J., Nicklas, H. E., MacQueen, P. J., Tejada, C., Cobos Duenas, F. J., & Mitsch, W. 1998, in *Society of Photo-Optical Instrumentation Engineers (SPIE) Conference Series*, Vol. 3355, Society of Photo-Optical Instrumentation Engineers (SPIE) Conference Series, ed. S. D'Odorico, 375-386
 Hillebrandt, W., & Niemeyer, J. C. 2000, *ARA&A*, 38, 191
 Höflich, P., Wheeler, J. C., & Thielemann, F.-K. 1998, *ApJ*, 495, 617
 Horne, K. 1986, *PASP*, 98, 609
 Howell, D. A. 2011, *Nature Communications*, 2
 Howell, D. A., et al. 2006, *Nature*, 443, 308
 Hoyle, F., & Fowler, W. A. 1960, *ApJ*, 132, 565
 Hsiao, E. Y., Conley, A., Howell, D. A., Sullivan, M., Pritchett, C. J., Carlberg, R. G., Nugent, P. E., & Phillips, M. M. 2007, *ApJ*, 663, 1187
 Jeffery, D. J., Leibundgut, B., Kirshner, R. P., Benetti, S., Branch, D., & Sonneborn, G. 1992, *ApJ*, 397, 304
 Jha, S., et al. 2006, *AJ*, 131, 527
 Jha, S., Riess, A. G., & Kirshner, R. P. 2007, *ApJ*, 659, 122
 Kasen, D. 2010, *ApJ*, 708, 1025
 Kessler, R., et al. 2009, *ApJS*, 185, 32
 Kirshner, R. P., et al. 1993, *ApJ*, 415, 589

- Kleiser, I., Cenko, S. B., Li, W., & Filippenko, A. V. 2009, Central Bureau Electronic Telegrams, 1918, 1
- Landolt, A. U. 1992, *AJ*, 104, 340
- Leibundgut, B., Kirshner, R. P., Filippenko, A. V., Shields, J. C., Foltz, C. B., Phillips, M. M., & Sonneborn, G. 1991, *ApJ*, 371, L23
- Lentz, E. J., Baron, E., Branch, D., & Hauschildt, P. H. 2001, *ApJ*, 557, 266
- Li, W., et al. 2003, *PASP*, 115, 453
- . 2001, *PASP*, 113, 1178
- Li, W., Jha, S., Filippenko, A. V., Bloom, J. S., Pooley, D., Foley, R. J., & Perley, D. A. 2006, *PASP*, 118, 37
- Mandel, K. S., Narayan, G., & Kirshner, R. P. 2011, *ApJ*, 731, 120
- Matheson, T., et al. 2000, *AJ*, 120, 1487
- Mazzali, P. A., et al. 2005, *ApJ*, 623, L37
- Miller, J. S., & Stone, R. P. S. 1993, *Lick Obs. Tech. Rep.* 66 (Santa Cruz: Lick Obs.)
- Milne, P. A., et al. 2010, *ApJ*, 721, 1627
- Navasardyan, H., Cappellaro, E., & Benetti, S. 2009, Central Bureau Electronic Telegrams, 1918, 2
- Nomoto, K., Thielemann, F.-K., & Yokoi, K. 1984, *ApJ*, 286, 644
- Nugent, P., Kim, A., & Perlmutter, S. 2002, *PASP*, 114, 803
- Oke, J. B., et al. 1995, *PASP*, 107, 375
- Parrent, J. T., et al. 2011, *ApJ*, 732, 30
- Perlmutter, S., et al. 1999, *ApJ*, 517, 565
- Pignata, G., et al. 2008, *MNRAS*, 388, 971
- Poole, T. S., et al. 2008, *MNRAS*, 383, 627
- Poznanski, D., Ganeshalingam, M., Silverman, J. M., & Filippenko, A. V. 2011, *MNRAS*, 415, L81
- Quimby, R., Brown, P., Gerardy, C., Odewahn, S. C., & Rostopchin, S. 2006, Central Bureau Electronic Telegrams, 393, 1
- Riess, A. G., et al. 1998, *AJ*, 116, 1009
- Riess, A. G., Filippenko, A. V., Li, W., & Schmidt, B. P. 1999, *AJ*, 118, 2668
- Riess, A. G., et al. 2007, *ApJ*, 659, 98
- Roming, P. W. A., et al. 2005, *Space Science Reviews*, 120, 95
- Sauer, D. N., et al. 2008, *MNRAS*, 391, 1605
- Schlegel, D. J., Finkbeiner, D. P., & Davis, M. 1998, *ApJ*, 500, 525
- Schmidt, G. D., Weymann, R. J., & Foltz, C. B. 1989, *PASP*, 101, 713
- Shetrone, M., et al. 2007, *PASP*, 119, 556
- Stritzinger, M., et al. 2002, *AJ*, 124, 2100
- Stritzinger, M., Suntzeff, N. B., Hamuy, M., Challis, P., Demarco, R., Germany, L., & Soderberg, A. M. 2005, *PASP*, 117, 810
- Strovink, M. 2007, *ApJ*, 671, 1084
- Suzuki, N., et al. 2011, *ArXiv e-prints*, 1105.3470
- Tully, R. B. 1988, Nearby galaxies catalog
- Wade, R. A., & Horne, K. 1988, *ApJ*, 324, 411
- Wang, X., et al. 2009a, *ApJ*, 699, L139
- . 2009b, *ApJ*, 697, 380
- Wong, O. I., et al. 2006, *MNRAS*, 371, 1855
- Wood-Vasey, W. M., et al. 2007, *ApJ*, 666, 694
- Woosley, S. E., Taam, R. E., & Weaver, T. A. 1986, *ApJ*, 301, 601